

CONFIDENTIAL

Copy 5
RM E52C04

NACA RM E52C04

NACA

RESEARCH MEMORANDUM

INVESTIGATION OF A 10-STAGE SUBSONIC AXIAL-FLOW

RESEARCH COMPRESSOR

II - PRELIMINARY ANALYSIS OF OVER-ALL
PERFORMANCE

By Ray E. Budinger and Arthur R. Thomson

CLASSIFICATION CHANGED
Lewis Flight Propulsion Laboratory
Cleveland, Ohio

UNCLASSIFIED

FOR REFERENCE

By authority of *RDCA* *RDCA*
RD-128

Date *June 24, 1958*

70118-12-58

CLASSIFIED DOCUMENT

NOT TO BE TAKEN FROM THIS ROOM

This material contains information affecting the National Defense of the United States within the meaning of the espionage laws, Title 18, U.S.C., Secs. 793 and 794, the transmission or revelation of which in any manner to an unauthorized person is prohibited by law.

NATIONAL ADVISORY COMMITTEE FOR AERONAUTICS

WASHINGTON
June 16, 1952

CONFIDENTIAL



NATIONAL ADVISORY COMMITTEE FOR AERONAUTICS

RESEARCH MEMORANDUM

INVESTIGATION OF A 10-STAGE SUBSONIC AXIAL-FLOW RESEARCH COMPRESSOR

II - PRELIMINARY ANALYSIS OF OVER-ALL PERFORMANCE

By Ray E. Budinger and Arthur R. Thomson


SUMMARY

An investigation of the over-all performance of a 20-inch-tip-diameter 10-stage compressor was conducted as the initial step in an investigation of the problems encountered in an axial-flow compressor having a high pressure ratio per stage. The compressor was designed to obtain a total-pressure ratio of 6.45 (corresponding to a root-mean total-pressure ratio per stage of 1.205) at an equivalent weight flow of 57.5 pounds per second (corresponding to a weight flow of 26.4 lb/sq ft of frontal area) at an equivalent tip speed of 869 feet per second.

The investigation was made over a range of weight flows at equivalent speeds from 30 to 110 percent of design speed. The compressor surge line was smooth and, combined with the high part-speed efficiency, could result in good performance, starting, and accelerating characteristics of an engine. The maximum total-pressure ratio obtained at design speed was 7.52 at an equivalent weight flow of 53.7 pounds per second with an adiabatic efficiency of 0.81. At design speed, a peak efficiency of 0.82 was obtained at an equivalent weight flow of 54.8 pounds per second and a total-pressure ratio of 7.20. At 110 percent of design speed, the maximum total-pressure ratio was 8.24 at an efficiency of 0.79 and an equivalent weight flow of 58.6 pounds per second. The peak efficiency curve was very flat over the entire speed range investigated, increasing from a value of 0.71 at 30 percent of design speed to a peak efficiency of 0.84 at approximately 85 percent speed and decreasing to 0.79 at 110 percent of design speed.

INTRODUCTION

The limited amount of research information available on the operation of high-stage-pressure-ratio multistage axial-flow compressors for application to aircraft engines indicates the need for research on this type of compressor. In order to investigate the problems that arise from compounding high performance stages, a 20-inch-tip-diameter 10-stage axial-flow compressor was designed and fabricated by the NACA Lewis



laboratory. The compressor was designed to achieve higher stage pressure ratios than those in current use while at the same time maintaining high mass flow and efficiency. The compressor was designed for a root-mean total-pressure ratio per stage of 1.205 with an equivalent weight flow of 26.4 pounds per second per square foot of frontal area.

As an initial step in the investigation, the over-all performance characteristics were obtained over a range of equivalent speeds from 30 to 110 percent of design speed. A preliminary analysis of the over-all performance was made on the basis of curves of total-pressure ratio, adiabatic temperature-rise efficiency, and average compressor-discharge Mach number plotted against equivalent weight flow. Stage and blade-row static-pressure ratios at the tip are presented in order to obtain a picture of the performance of the individual stages over the speed and weight flow ranges investigated.

SYMBOLS

The following symbols are used in this report:

A	frontal area, sq ft
C_L	lift coefficient of an isolated airfoil
N	compressor speed, rpm
P	absolute total pressure, lb/sq ft
p	absolute static pressure, lb/sq ft
U	tip speed, ft/sec
V	axial velocity, ft/sec
$W/\bar{\theta}/\delta$	weight flow corrected to NACA standard sea-level conditions, lb/sec
$W/\bar{\theta}/A\delta$	specific weight flow corrected to NACA standard sea-level conditions, (lb/sec)/sq ft of frontal area
α	angle of attack, deg
δ	ratio of inlet total pressure to NACA standard sea-level pressure
θ	ratio of inlet total temperature to NACA standard sea-level temperature
σ	blade element solidity, ratio of chord length to circumferential distance between adjacent blades

Subscripts:

n	station number
0	inlet depression tank
1,3,5,...19	stations ahead of rotors of 1,2,...10 stages
2,4,6,...20	stations ahead of stators of 1,2,...10 stages
21	station ahead of discharge vanes
22	station behind discharge vanes
23	station in diffuser

APPARATUS

Compressor. - A cross-sectional view of the compressor, inlet bell-mouth, and discharge collector is shown in figure 1.

The compressor blading was designed for a symmetrical velocity diagram and constant total enthalpy at all radii with simple radial equilibrium of static pressure and centrifugal force after each blade row. Reference 1 shows that this type of velocity diagram and enthalpy distribution produces a higher pressure ratio and mass flow for a given Mach number and blade loading limitation than the conventional vortex velocity diagram.

The details of the aerodynamic design of the compressor are presented in reference 2. The important design criteria are as follows:

Number of stages	10
Constant tip diameter, in.	20
Hub to tip ratio at first rotor inlet.	0.55
Axial velocity to tip speed ratio at hub of first rotor.	0.75
Solidity at hub of each blade row, σ	1.10
Turning limitation, α_{CL}	
for stages 1 to 3.	0.8
for stages 4 to 6.	0.9
for stages 7 to 10	1.0
Relative inlet Mach number at hub of each rotor.	0.70
Polytropic stage efficiency.	0.90

The design performance values for the compressor are as follows:

Total-pressure ratio	6.45
Root-mean total-pressure ratio per stage	1.205
Equivalent weight flow, lb/sec	57.5
Equivalent weight flow, (lb/sec)/sq ft of frontal area	26.4
Equivalent tip speed, ft/sec	869
Average compressor-discharge Mach number	0.55

Installation. - The compressor was driven by a 9000-horsepower variable-frequency electric motor. The speed was maintained constant by an electronic control and was measured by an electric chronometric tachometer.

Air entered through a calibrated, adjustable submerged orifice and a butterfly inlet throttle into a depression tank 6 feet in diameter and approximately 10 feet long. Screens in the depression tank and a smooth bellmouth faired into the compressor inlet insured a uniform distribution of air entering the compressor. Air was discharged from the compressor into a collector that was connected to the laboratory altitude exhaust system. Air weight flow was controlled by a butterfly valve located in the exhaust ducting. The compressor was insulated with 2 inches of glass wool in order to reduce the heat loss through the casing.

Instrumentation. - The location of the compressor instrumentation in the depression tank and at the compressor discharge is shown in figure 1. The axial locations of the instrument measuring stations were in accordance with the recommendations of reference 3. Radial distributions of total temperature and total pressure were obtained from multiple rakes located at area centers of equal areas. The instruments used at each station and the methods of measurement were as follows:

Compressor-inlet pressure	Four wall static pressure taps 90° apart and two shielded total pressure probes.
Compressor-inlet temperature	Five multiple tip total temperature probes.
Compressor-blade-row static pressures	Four wall static pressure taps located around the circumference after each blade row.
Compressor-discharge pressure	Four wall static pressure taps and three 10-tube circumferential total-pressure rakes (fig. 2(a)).
Compressor-discharge temperature	One spike-type thermocouple rake (fig. 2(b)) with three measuring stations. Four spike-type thermocouple rakes with four measuring stations were located 11 inches downstream of the discharge vanes in the diffuser.

Pressure measurement	Water and mercury manometers.
Temperature measurement	Calibrated potentiometer in conjunction with a spotlight galvanometer.

The accuracy of measurement is estimated to be within the following limits:

Temperature, °F	±1.0
Pressure, in. Hg.	±0.05
Weight flow, percent.	±1.5
Speed, percent.	±0.3

PROCEDURE

Operation. - The compressor was operated at equivalent speeds corresponding to 30, 50, 60, 70, 80, 90, 100, and 110 percent of design speed. At each speed, a range of air flows was investigated from a flow at which surge occurred to a limiting flow at which the compressor was choked. The inlet pressure was varied to maintain a constant Reynolds number of approximately 190,000 relative to the first rotor at the tip at all speeds except 30 percent of design speed. Atmospheric air was used at all speeds except 110 percent of design speed where refrigerated air was used in order to reduce the actual compressor speed.

Calculation. - At each flow point, the discharge total pressure was obtained by two methods. The measured total pressure is the arithmetic average of the circumferential rake measurements at three radial positions. The calculated total pressure was obtained by the method presented in reference 3. Adiabatic temperature-rise efficiencies were calculated by use of both the measured and the calculated total-pressure ratios in the determination of the isentropic power input. The arithmetic average of the radial temperature readings measured by the single thermocouple rake at the compressor discharge was used in the determination of the actual power input. The close agreement in total temperature measured with the discharge rake and with the thermocouple rakes in the diffuser justified the use of the single probe for the efficiency calculations.

The calculated discharge total pressure does not consider radial or circumferential discharge velocity gradients or deviation from the axial direction. Consequently, the calculated total-pressure ratio and efficiency will be lower than the measured values. These values are conservative, but are felt to be a truer measure of the recoverable energy at the compressor discharge. All numerical values presented in the text of the report are based on the calculated discharge total pressure.

RESULTS

The over-all performance characteristics of the compressor are presented in figure 3 as a plot of total-pressure ratio with contours of constant efficiency as a function of equivalent weight flow over a range of equivalent speeds from 30 to 110 percent of design speed. A comparison between the measured and calculated values of total-pressure ratio and efficiency is presented in figures 4 to 6.

The maximum total-pressure ratio obtained at design speed was 7.52 (fig. 3) at an equivalent weight flow of 53.7 pounds per second with an efficiency of 0.81 (fig. 6). The peak efficiency of 0.82 at design speed occurred at a total-pressure ratio of 7.20 and an equivalent weight flow of 54.8 pounds per second. At 110 percent of design speed, the maximum total-pressure ratio was 8.24 at an equivalent weight flow of 58.6 pounds per second with an efficiency of 0.79. The compressor surge line (fig. 3) was very smooth, having a steadily increasing slope up to design speed at which point the slope began to decrease slightly. The regions of relatively high efficiency extended well into the low-speed operating range of the compressor. At the higher equivalent speeds, the efficiency contours were very broad, which indicated a wide operating range of approximately constant efficiency. The peak efficiency line based on calculated total pressure (fig. 6) was unusually flat over the entire speed range, increasing from a value of 0.71 at 30 percent of design speed to a maximum value of 0.84 at approximately 85 percent speed and decreasing to 0.79 at 110 percent of design speed.

The differences between the performance as determined from the measured and calculated values of discharge total pressure are clearly evidenced on figures 4 to 6. The differences in the curves give an indication of the flow deviations from the axial direction and of the nonuniformity of the discharge velocity.

The agreement between the two methods is best at the low-flow end of the individual speed curves and improves over the weight flow range as the speed is increased. At a given speed, the blade wakes and losses at the walls are greatest at the high-flow end of the curve, which probably accounts for the greater discrepancy in that region of the curve. At low speeds, mismatching of the individual blade rows resulted in large regions of total pressure defect. This defect is a larger percentage of the discharge total pressure at low speeds than at high speeds; consequently, the discrepancy between the measured and calculated curves will decrease as the speed increases.

DISCUSSION OF RESULTS

2517 Part-speed efficiency. - The high part-speed efficiency of the compressor may be attributed to several factors in the aerodynamic design. These factors are discussed primarily as they affect the inlet stage, since over the speed range investigated this stage is required to operate over the widest range of angle of attack and can therefore be considered the most critical stage in the compressor. The following three factors are probably most important in contributing to the relatively constant efficiency obtained over a wide range of speeds:

1. For a symmetrical velocity diagram the low design value of turning limitation σC_L for the inlet stage permitted the increased turning required by the high angles of attack at part speed without an appreciable reduction in stage efficiency.
2. The design limitations and type of velocity diagram selected resulted in low values of relative inlet air angle measured with respect to the axial direction. A given change in axial velocity has less effect on the angle of attack for a low inlet air angle design than for a high inlet air angle design. The low values of relative inlet air angle also result in small tangential velocity components which reduce the radial gradient of static pressure and therefore probably reduce secondary flow losses.
3. Another factor which may contribute to the good part-speed efficiency of the compressor was the selection of a constant-camber blade section at all radii of a given blade row. The camber of each blade row was selected to give design angle of attack near the pitch radius, while departing slightly at the hub and tip from the optimum design values. This selection reduced the angle of attack at the tip below the optimum design value and tended to delay tip stall at part speed. Single-stage research has shown that the tip blade section will stall first for a compressor designed with a symmetrical velocity diagram and constant total enthalpy at all radii. This tip stall will be less critical for a low tip speed design than for a high tip speed design. The stall condition at the tip shifts the mass flow toward the hub and thus reduces the tendency of the hub to stall. This progressive type of stall from tip to hub may be advantageous to part-speed performance since the tip section may be stalled while the remainder of the blade will be utilized efficiently.

Surge characteristics. - A reproduction of the over-all performance curve with a typical engine operating line computed to pass through the regions of maximum efficiency is presented in figure 7. The operating line was obtained by use of the general equations for compressor and turbine matching. These equations require that continuity be satisfied through the engine, that the turbine power be equal to that required to drive the compressor, and that the pressure rise through the inlet diffuser and compressor must equal the pressure drop through the burner, turbine, and jet nozzle.

The surge line and the operating line are approximately parallel, which means that the high pressure ratio, efficiency, and weight flow at design speed can be utilized effectively in an engine. Because the surge and operating lines are parallel, the operating line does not pass through the surge region. Also the shape of this operating line allows a good margin for acceleration at all speeds. Thus the smooth surge line of this compressor, combined with the high part-speed efficiencies when properly matched with a turbine, could produce an engine with very good performance, starting, and accelerating characteristics.

Overspeed characteristics. - Altitude operation at cruising flight speeds requires compressor equivalent speeds higher than design; consequently, it is desirable to maintain high efficiency at overspeed. The peak efficiency at 110 percent of design speed dropped to 0.79 with only a small increase in equivalent weight flow over the design-speed weight flow. These factors indicate that the compressor was designed very near its Mach number limit at design speed with little margin for altitude operation. The reduction in efficiency and the choking of the compressor were probably caused by local sonic velocities in the inlet stages. At overspeed the angle of attack on the inlet stages is decreased below the design value. If the angle of attack decreases enough, negative stall will occur and produce flow separation on the pressure surface of the blade. This separated flow causes an effective reduction in area which may increase the local velocity to the speed of sound. Another possibility of attaining a local Mach number equal to 1 could be due to exceeding the critical Mach number of the blade section.

In view of the decrease in compressor performance at 110 percent of design speed, the ideal match point for a turbine to produce an engine with good altitude operating characteristics would be approximately 90 percent of design speed. This speed would be selected on the basis of the high efficiency obtained with a reasonably high total pressure ratio, combined with the good compressor performance obtained at speeds above 90 percent of design.

Compressor discharge Mach number. - The average compressor-discharge Mach number is presented in figure 8 plotted against equivalent weight flow over the range of equivalent speeds investigated. The shape of the surge line on figure 8 indicates that along the surge line the discharge velocity increases faster than the speed of sound up to 70 percent of design speed, which results in an increasing Mach number. The velocity of sound is a function of the static temperature ratio and will increase as the compression ratio across the compressor increases. Above 70 percent of design speed, the increase in compression ratio is greater than the increase in discharge velocity, which results in a decreasing discharge Mach number.

The compressor design discharge Mach number was 0.55, which gives a discharge velocity of 795 feet per second. The most desirable point of compressor operation at design speed would be at peak efficiency. At this point the discharge Mach number was 0.45 with a velocity slightly over 700 feet per second. This value of discharge velocity is high and may present a problem in diffusing to a reasonable combustor-inlet velocity. Combustor research (reference 4) indicates that combustor efficiency improves with increasing values of inlet static pressure and total temperature and with decreasing values of velocity. The high static pressure and total temperature at the discharge of a high-pressure-ratio compressor coupled with a practical diffuser will allow higher discharge velocities and still produce acceptable combustor performance.

Stage characteristics. - A typical single-stage compressor curve of static-pressure ratio is plotted in figure 9 against a weight flow parameter which is proportional to the axial velocity divided by tip speed. The peak pressure ratio and a typical peak efficiency point are indicated on the curve. The direction of increasing angle of attack and positive stall is to the left of the peak-pressure-ratio point and the direction of decreasing angle of attack and negative stall is to the right. In multistage compressor design, the blading for each stage at the design point is usually selected to operate at the peak efficiency point of the stage performance curve, as indicated on figure 9.

In multistage compressors at part speed, the inlet stages are operating well on the positive stall side of the stage performance curve. Each succeeding stage operates at a progressively increasing value of V/U . The intermediate stages operate very near their design point, whereas the latter stages have moved beyond the design point toward the negative stall side of the stage performance curve. Thus some of the stages must operate far from their respective design points at part speed.

As design speed is approached, the inlet stages move to higher values of V/U . The intermediate stages do not move far from their design point because the density increase through the inlet stages compensates for the increased weight flow. The latter stages move toward their design points because the effect of density increase is greater than the effect of increased weight flow. Thus as design speed is approached theoretically, all stages converge on their respective design points. This effect continues above design speed at an accelerated rate, causing mismatching of the stages.

Some of the effects of stage characteristics on the performance of a multistage compressor can now be enumerated:

1. The typical stage performance curve (fig. 9) shows that stages operating in the region of negative stall impose a limit on the mass

flow. Therefore from the previous analysis at part speed, the latter stages, and at overspeed the inlet stages, limit the maximum weight flow obtained at a given speed.

2. At off-design conditions the inlet and exit stages must operate away from their design points. These stages must have a sufficient range of good operation, while the intermediate stages require a narrower range of good operation. Thus, the individual stage characteristics directly affect the performance and matching of a multistage compressor.

Representative stage performance curves shown in figure 10 demonstrate the trends described previously. The operating range of the inlet stage obtained at each speed can be considered as a segment of the typical stage performance curve (fig. 9). At speeds up to and including 70 percent of design speed, the inlet stage operates on the positive stall side of the peak pressure ratio point. At 80 percent speed the stage is operating at approximately the peak-pressure-ratio point. At 90 percent speed and above, the inlet stage moves toward the negative stall side of the stage performance curve.

The intermediate stage (fifth) at low speeds operates at approximately peak pressure ratio (fig. 10). Near design speed (90 and 100 percent) this stage moves slightly toward the negative stall region. Because the exit stage operates on the negative stall side of figure 9, a change in compressor weight flow has considerable effect on its performance. A reduction in weight flow at all speeds moves the exit stage toward its peak-pressure-ratio point. Likewise as design speed is approached, this stage operates nearer its peak pressure ratio.

At low speeds the exit stage is operating near choke and is limiting the mass flow of the compressor. At design speed all stages are operating on the negative stall side of the stage performance curve at high weight flow and the stage which reaches its choke point first will limit the weight flow. At overspeed, some stage between the first and fifth has moved to the choke point since no range of static-pressure ratio was obtained on the inlet stage, whereas a small range was obtained on both the intermediate and exit stages.

On figure 11 the over-all static-pressure ratio, the stage static-pressure ratio, and the blade-row static-pressure ratio are compared with the design values at approximately the design point. Reasonably good agreement was obtained.

The compressor design (reference 2) made no allowance for boundary-layer build-up along the hub and outer casing, which would have effectively moved the design point to a lower weight flow. This boundary-layer build-up affects the radial distribution of axial velocity through the compressor and hence the pressure ratio. Apparently, in actual

operation the flow is being overturned by the individual stages as shown by the higher values of static-pressure ratio in figures 11(a) and 11(b), respectively. However in the inlet stage, there is underturning of the rotor, as shown in figure 11(c). The boundary layer effectively reduces the flow area and thus increases the axial velocities, while the overturning of the flow tends to reduce the axial velocities. Consequently, the presence of the boundary layer probably increases the maximum permissible turning and results in higher pressure ratios at design speed without exceeding the blade loading limitations.

SUMMARY OF RESULTS

The following results were obtained from an investigation of overall performance of the 10-stage axial-flow compressor:

1. The compressor surge line was smooth, and combined with the high part-speed efficiency of the compressor could result in good performance, starting, and accelerating characteristics of an engine.
2. The maximum total-pressure ratio obtained at design speed was 7.52 at an equivalent weight flow of 53.7 pounds per second with an efficiency of 0.81.
3. A peak efficiency of 0.82 was obtained at design speed with a total-pressure ratio of 7.20 and an equivalent weight flow of 54.8 pounds per second.
4. At 110 percent of design speed, the maximum total-pressure ratio was 8.24 at an efficiency of 0.79 and an equivalent weight flow of 58.6 pounds per second.
5. The compressor had an unusually flat peak efficiency curve over the range of speeds investigated, increasing from a value of 0.71 at 30 percent of design speed to a peak efficiency of 0.84 at approximately 85 percent of design speed and decreasing to a value of 0.79 at 110 percent of design speed.

Lewis Flight Propulsion Laboratory
National Advisory Committee for Aeronautics
Cleveland, Ohio

REFERENCES

1. Voit, Charles H., and Thomson, Arthur R.: An Analytical Investigation Using Aerodynamic Limitations of Several Designs of High Stage Pressure Ratio Multistage Compressors. NACA TN 2589, 1951.
2. Johnsen, Irving A.: Investigation of a 10-Stage Subsonic Axial-Flow Research Compressor. I - Aerodynamic Design. NACA RM E52B18, 1952.
3. NACA Subcommittee on Compressors: Standard Procedures for Rating and Testing Multistage Axial-Flow Compressors. NACA TN 1138, 1946.
4. Olson, Walter T., and Childs, J. Howard: NACA Research on Combustors for Aircraft Gas Turbines. I - Effect of Operating Variables on Steady-State Performance. NACA RM E50H31, 1950.

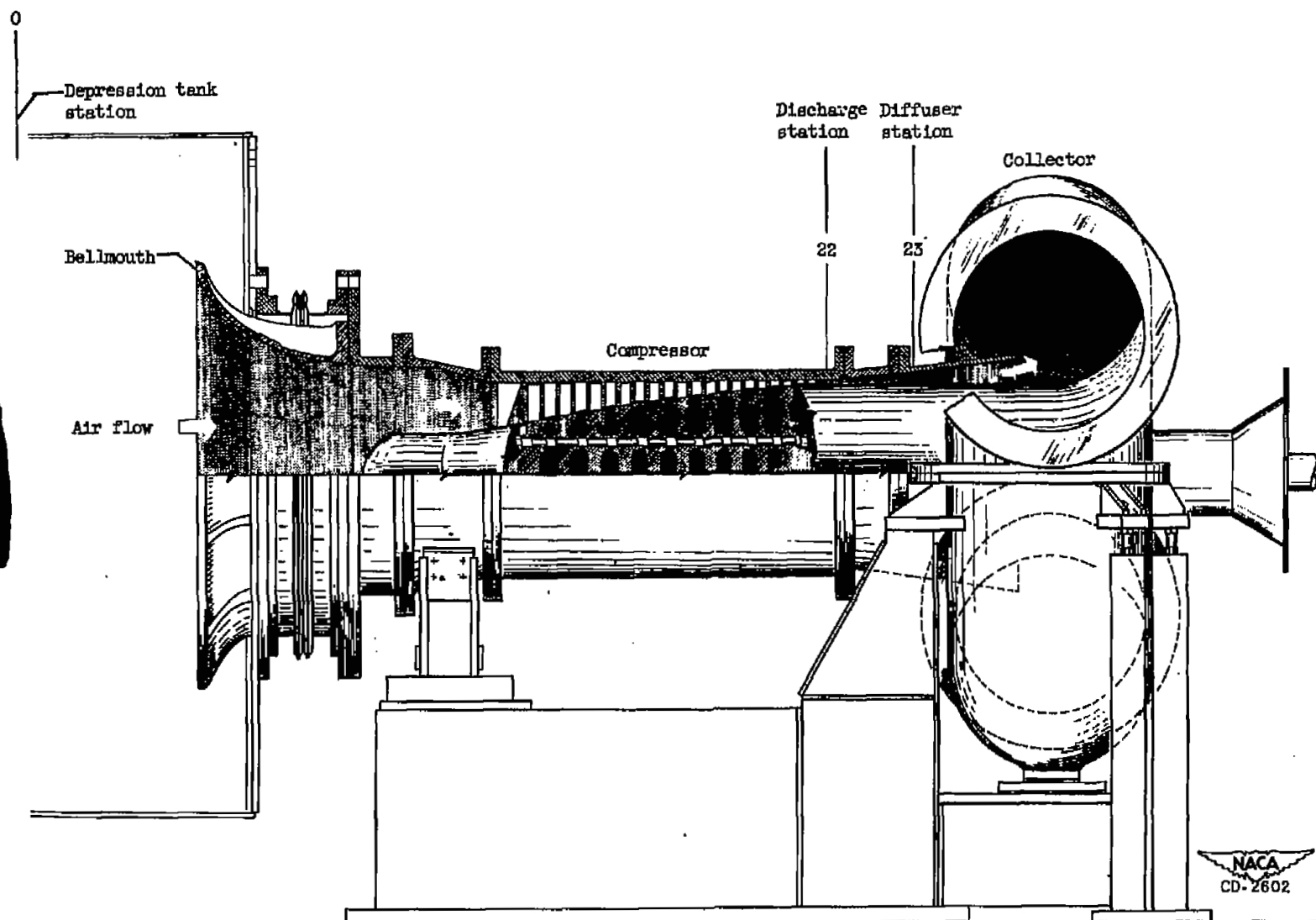
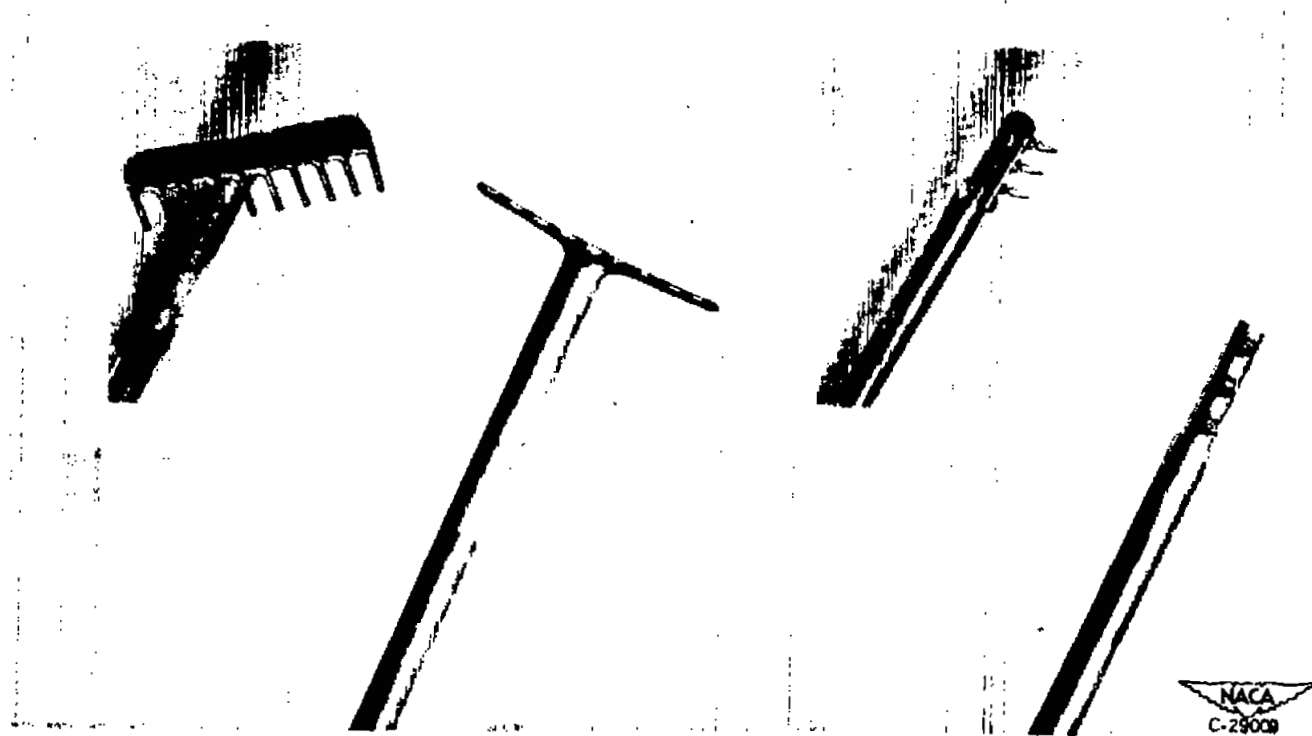


Figure 1. - Cross-section view of 10-stage compressor, inlet bellmouth, and discharge collector.



(a) Total pressure rake.

(b) Spike-type thermocouple rake.



Figure 2. - Compressor-discharge instrumentation.

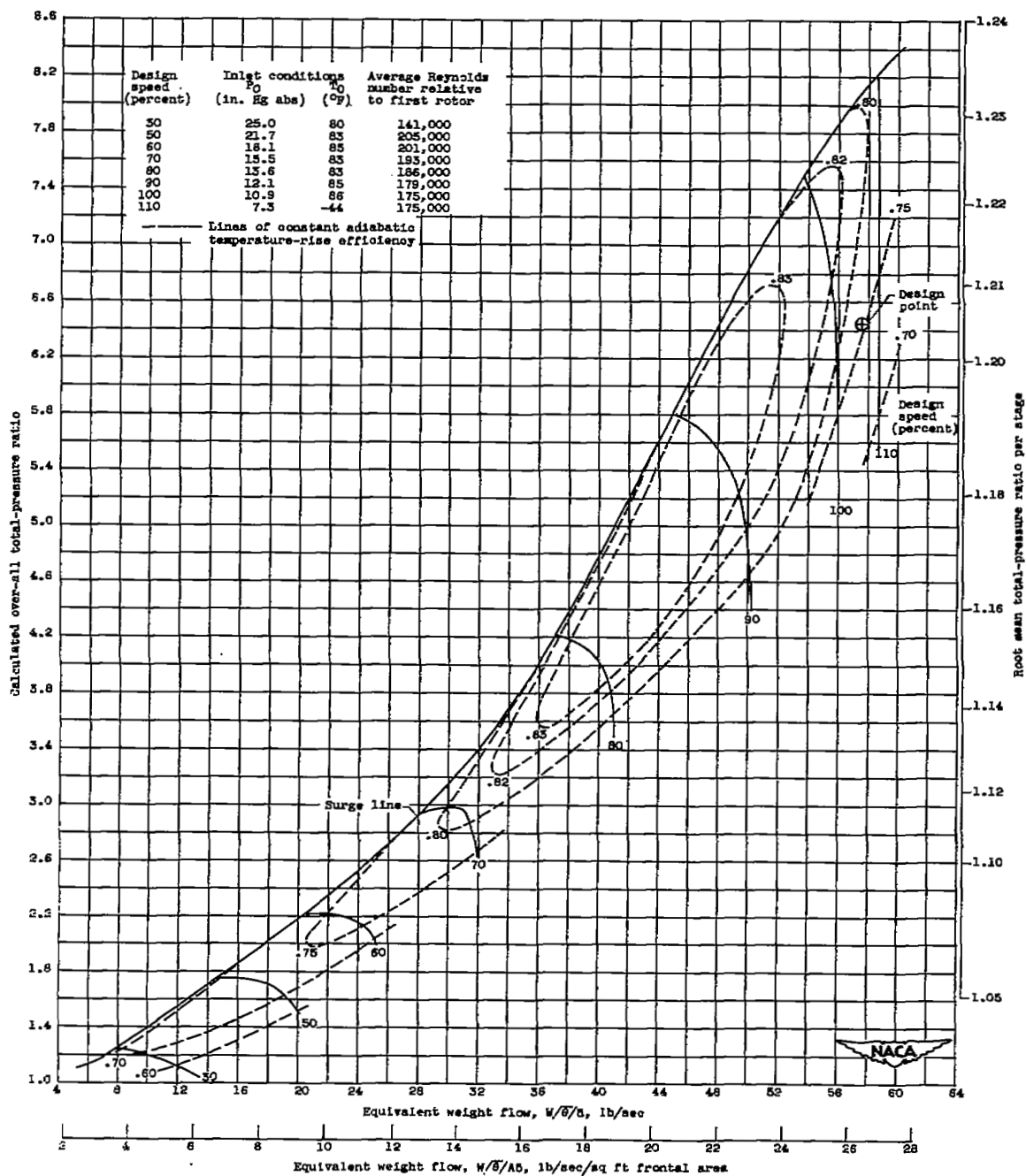


Figure 3. - Over-all performance characteristics of 10-stage axial-flow compressor.

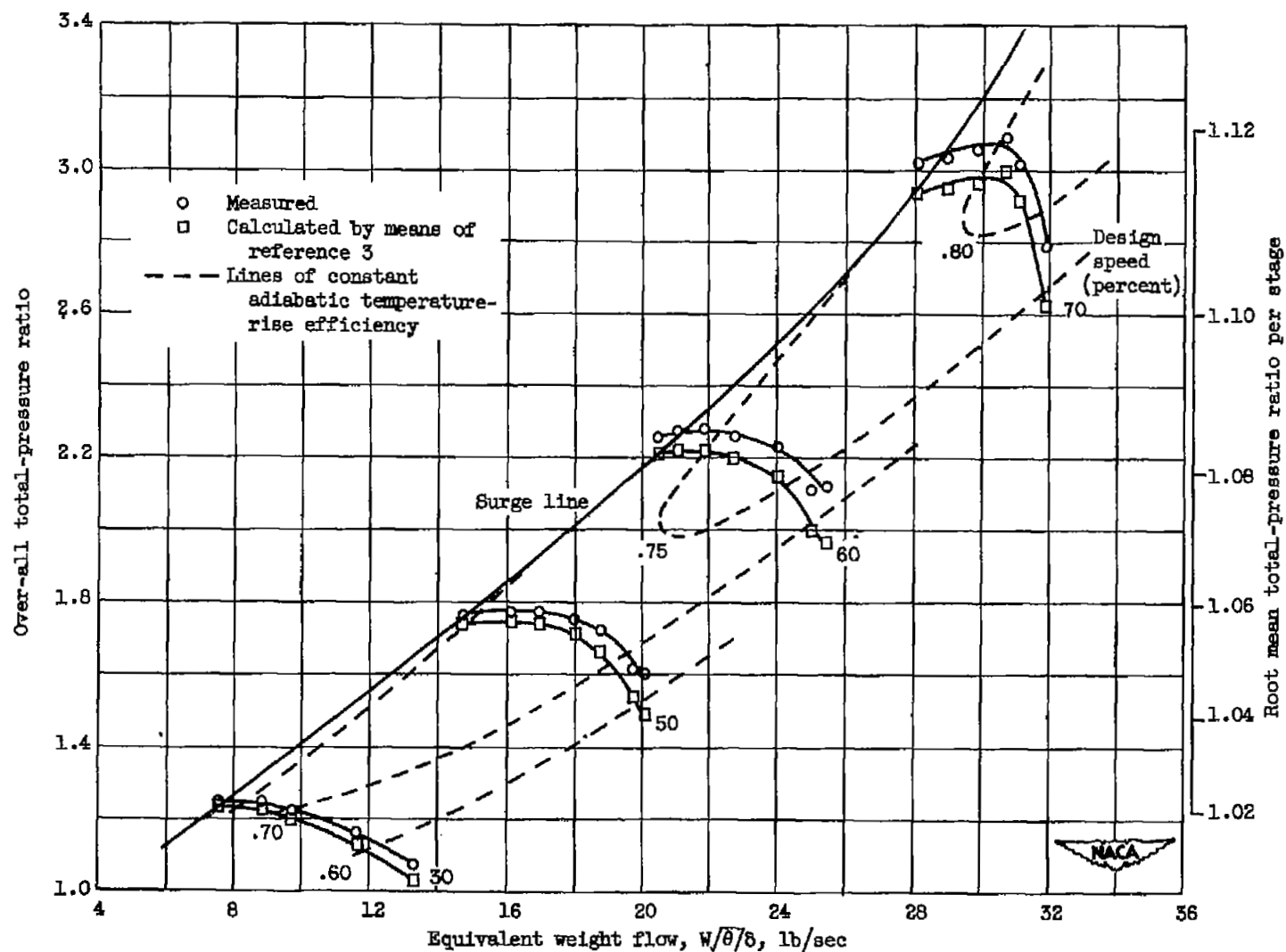


Figure 4. - Over-all performance characteristics at low speeds.

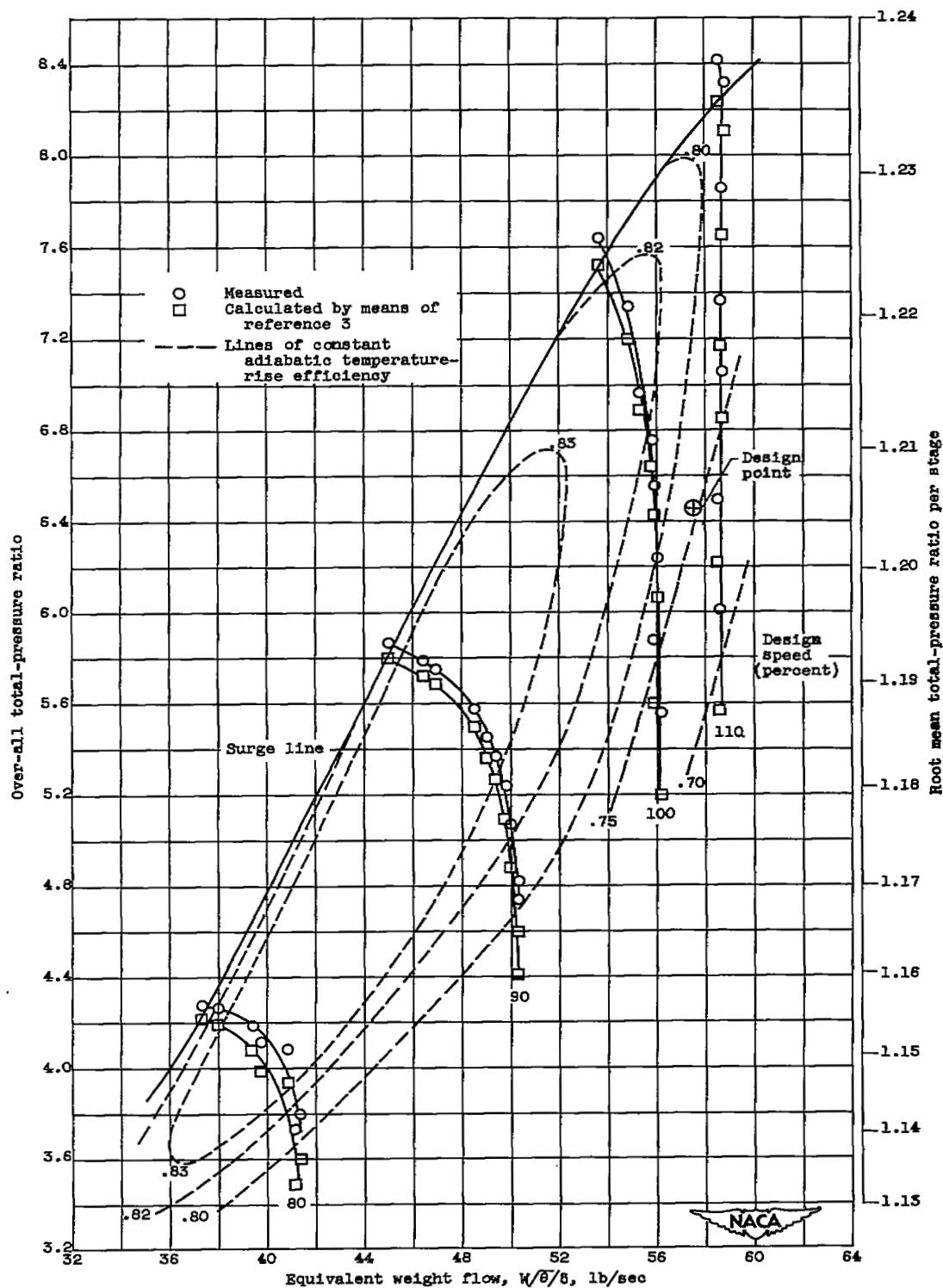


Figure 5. - Over-all performance characteristics at high speeds.

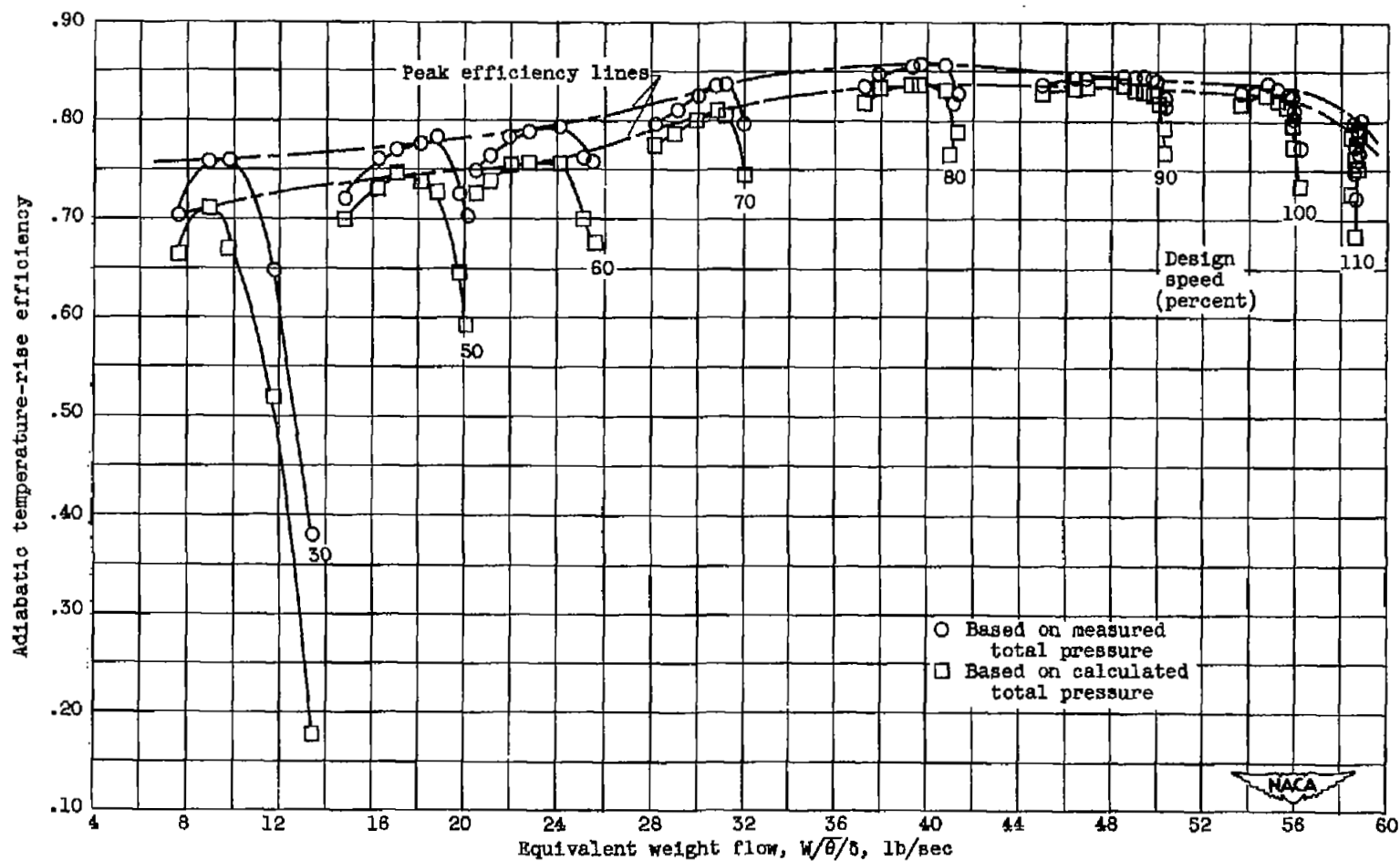


Figure 6. - Variation of adiabatic temperature-rise efficiency with speed and weight flow.

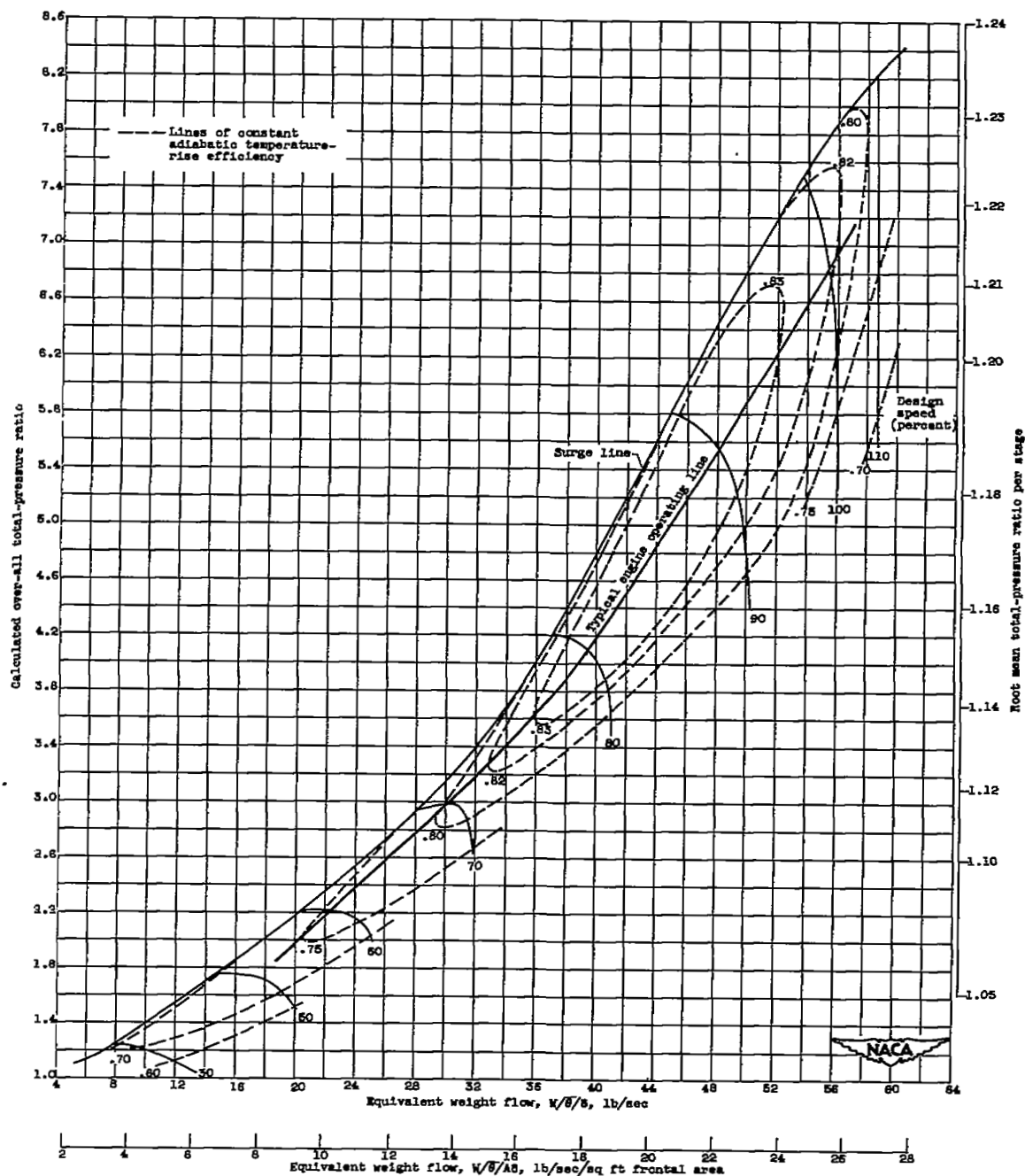


Figure 7. - Over-all performance characteristics with typical engine operating line superimposed.

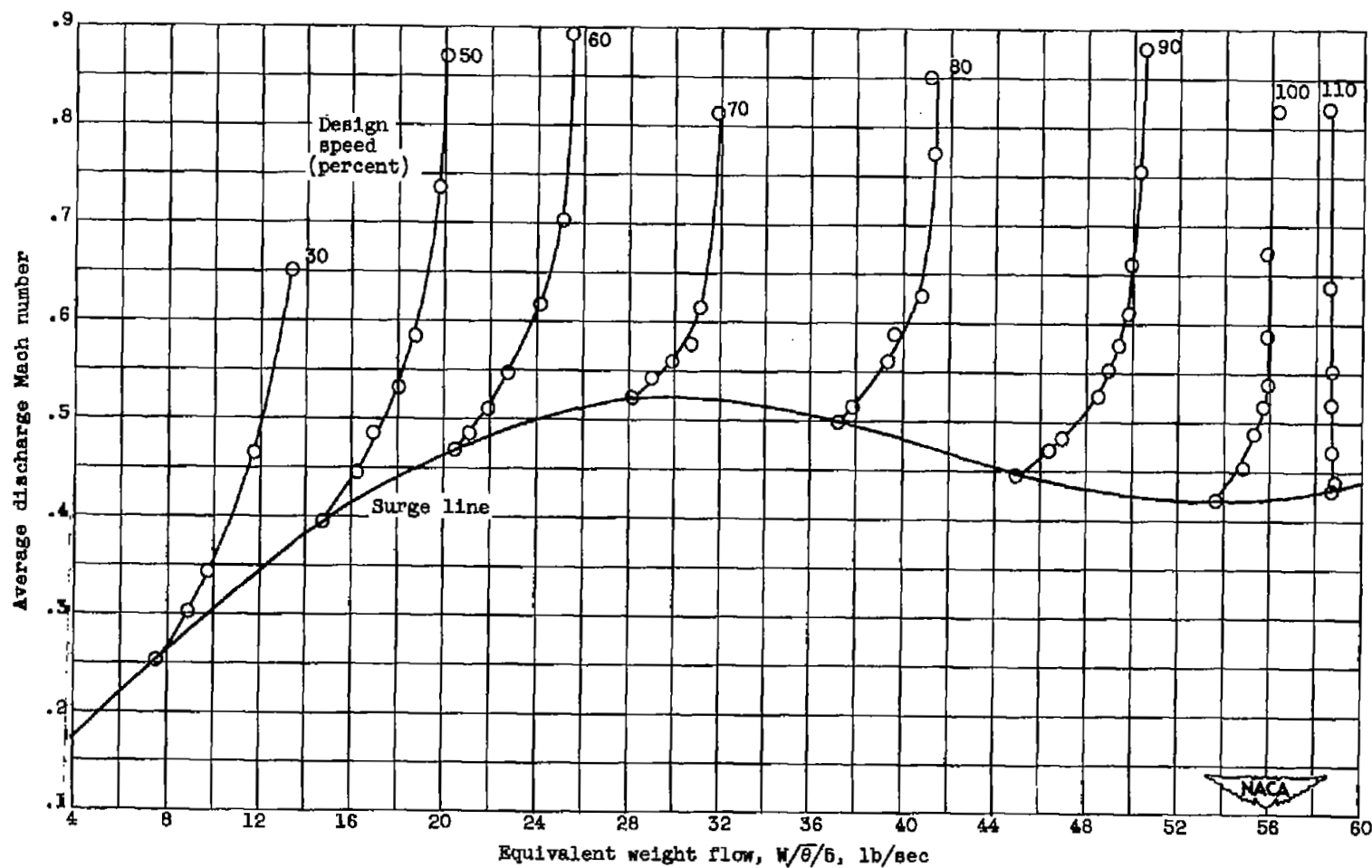


Figure 8. - Variation of average discharge Mach number with speed and weight flow.

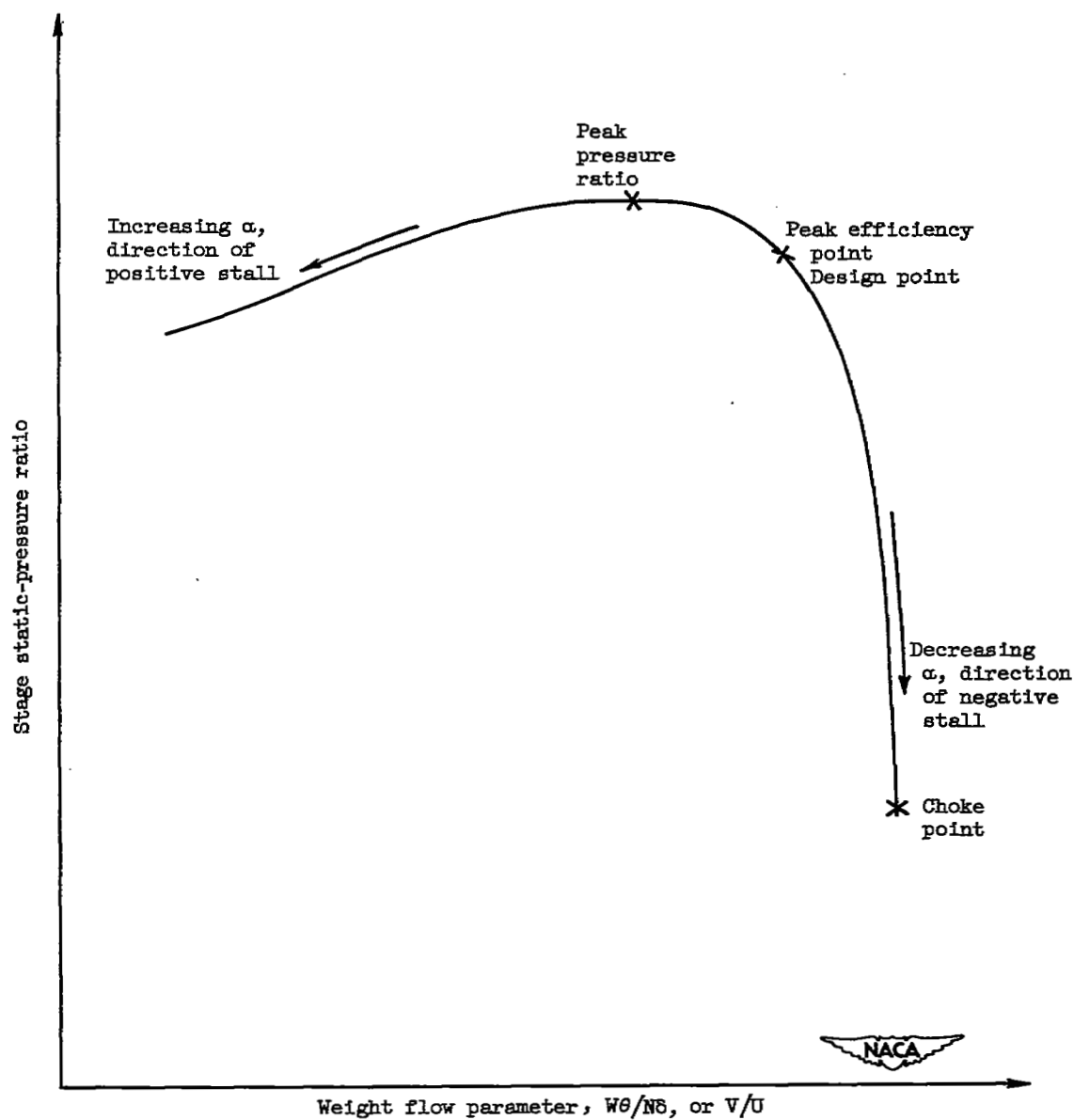


Figure 9. - Typical stage performance curve.

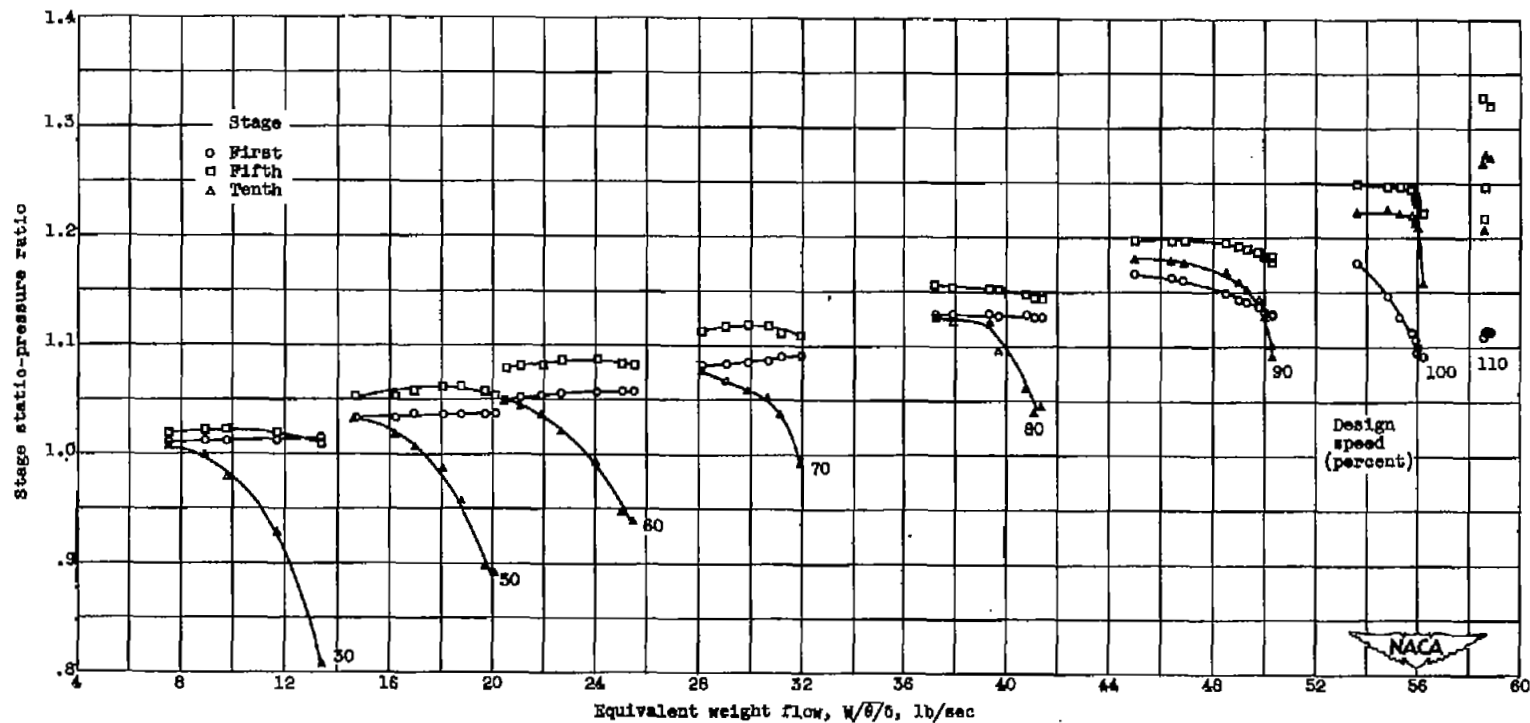
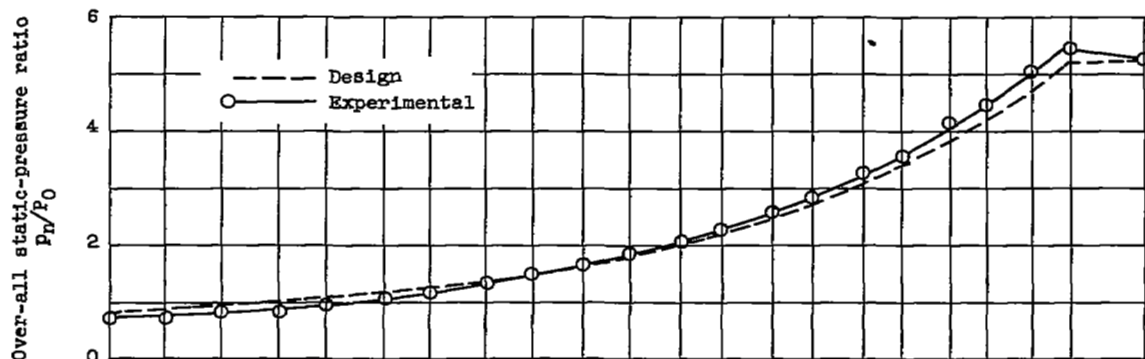
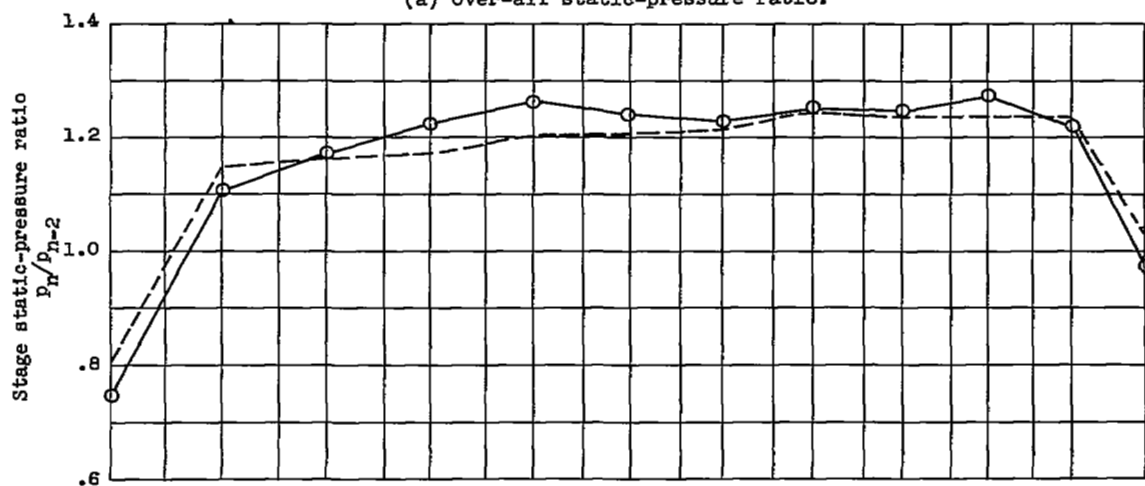


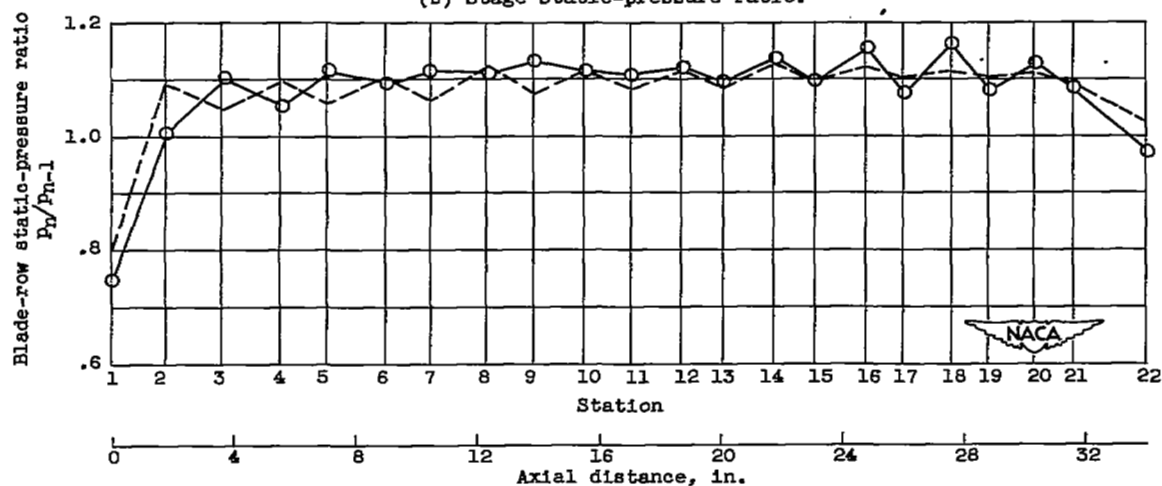
Figure 10. - Variation of stage static-pressure ratio across first, fifth, and tenth stages with speed and weight flow.



(a) Over-all static-pressure ratio.



(b) Stage static-pressure ratio.



(c) Blade-row static-pressure ratio.

Figure 11. - Comparison with design of static-pressure ratio distribution obtained at approximately design over-all total-pressure ratio.

SECURITY INFORMATION

NASA Technical Library



3 1176 01436 0052

